IEEE Access
Multidisciplinary | Rapid Review | Open Access Journal

Received August 22, 2019, accepted October 12, 2019, date of publication October 18, 2019, date of current version October 30, 2019.

Digital Object Identifier 10.1109/ACCESS.2019.2948317

Robust Unscented Kalman Filtering With Measurement Error Detection for Tightly Coupled INS/GNSS Integration in Hypersonic Vehicle Navigation

GAOGE HU[1], BINGBING GAO[1], YONGMIN ZHONG[2], LONGQIANG NI[3], AND CHENGFAN GU[2]

[1]School of Automation, Northwestern Polytechnical University, Xi'an 710072, China
[2]School of Aerospace, Mechanical and Manufacturing Engineering, RMIT University, Melbourne, VIC 3000, Australia
[3]Northwest Institute of Mechanical and Engineering, Xianyang 100084, China

Corresponding author: Gaoge Hu (hugaoge1111@126.com)

This work was supported in part by the Fundamental Research Funds for the Central Universities under Project 3102018zy027, and in part by the National Natural Science Foundation of China under Project 61703424 and Project 41904028.

ABSTRACT Due to the high maneuverability of a hypersonic vehicle, the measurements for tightly coupled INS/GNSS (inertial navigation system/global navigation satellite system) integration system inevitably involve errors. The typical measurement errors include outliers in pseudorange observations and non-Gaussian noise distribution. This paper focuses on the nonlinear state estimation problem in hypersonic vehicle navigation. It presents a new innovation orthogonality-based robust unscented Kalman filter (IO-RUKF) to resist the disturbance of measurement errors on navigation performance. This IO-RUKF detects measurement errors by use of the hypothesis test theory. Subsequently, it introduces a defined robust factor to inflate the covariance of predicted measurement and further rescale the Kalman gain such that the measurements in error are less weighted to ensure the filtering robustness against measurement errors. The proposed IO-RUKF can not only correct the UKF sensitivity to measurement errors, but also avoids the loss of accuracy for state estimation in the absence of measurement errors. The efficacy and superiority of the proposed IO-RUKF have been verified through simulations and comparison analysis.

INDEX TERMS INS/GNSS integration, robust unscented Kalman filter, measurement errors, hypersonic vehicle navigation.

I. INTRODUCTION

Hypersonic vehicle refers to a vehicle at the speed of Mach 5 or above. Due to the merits such as large flight envelope, high maneuverability and speedy global reach, hypersonic vehicle has received great attention in the recent years in both aeronautic and astronautic fields for various civil and military applications [1], [2]. As the ''eye'' of a hypersonic vehicle, the navigation system is the primary element of the overall vehicle flight control system (navigation, guidance and control system). The position, speed and attitude information provided by the navigation system is directly related to the accuracy and reliability of the vehicle guidance and control loop [3].

The associate editor coordinating the review of this manuscript and approving it for publication was Masood Ur-Rehman.

Nowadays, the INS/GNSS (inertial navigation system/global navigation satellite system) integration has been a widely used navigation technique for hypersonic vehicles [4], [5]. The integration of INS and GNSS overcomes the limitations of both standalone systems, i.e., the growth of navigation errors with time for INS as well as the typical low update rate of GNSS measurements. Thus, it can provide a superior performance comparing to either INS or GNSS [6]–[8]. The integration of INS and GNSS can be classified into two categories [9]–[11]. One is the loosely coupled integration which employ the velocity and position estimations solved by GNSS to assist INS. This method is simple in principle and easy to implement. However, the number of observable GNSS satellites frequently drops to below four due to high maneuverability, leading to the poor stability and reliability. Thus, the method is

unsuitable for hypersonic vehicle navigation. This problem can be easily addressed by the tightly coupled integration in which the raw GNSS pseudorange measurements is directly used as measurements to update the navigation filtering. The tightly coupled integration can also refrain from the loss of information and cross correlation of position estimates involved in the loosely coupled integration [9]. Nevertheless, the tightly coupled INS/GNSS integration incorporates nonlinearity in the measurement model due to the nonlinear nature of GNSS pseudorange. As a result, a nonlinear Kalman filtering method is required for navigation sensor fusion [10].

The extended Kalman filter (EKF) is a typically employed method in the integration of INS and GNSS [12]. It is an approximation method, in which nonlinear system models are truncated through the first-order Taylor expansion such that the Kalman filter can be applied. Although the EKF has the advantage in real-time estimation, the linearization of system model may cause a biased or even divergent filtering solution [13], [14]. The deterministic sampling based unscented Kalman filter (UKF) is proposed as an improvement to EKF. It uses a finite number of sigma points to capture high-order system characteristics, leading to a better performance than EKF in terms of both estimation accuracy and convergence [15]. However, similar to EKF, the performance of UKF depends on the pre-defined process and measurement models of a dynamical system. If the system models involve uncertainties, UKF will generate poor solutions [16]–[18]. As to the INS/GNSS integrated system for hypersonic vehicle navigation, because the GNSS receiver is easily affected by abnormal interference during highly dynamic maneuvers, the measurements inevitably involve errors such as typical outliers in pseudorange observations and non-Gaussian characteristics of noise statistics [12], [19]. Therefore, it requires UKF to counteract the above measurement errors involved in INS/GNSS integration for hypersonic vehicle navigation.

Various robust UKFs were reported to handle both outliers and non-Gaussian measurement noises in nonlinear systems. The robust UKFs based on the MIT principle [20], covariance matching [18], maximum likelihood criterion [21] and moving window [13], treat measurement errors as inaccurate noise statistics to improve the UKF robustness by online estimating noise statistics. Nevertheless, these methods face the following twofold shortcomings in practical application. Firstly, the "rank deficient" issue is likely to occur in the calculation of noise statistics for a high-dimensional system, leading to the stability issue. Secondly, the estimation of noise statistics based on historical residuals is of hysteresis, leading to the difficulty to adapt to highly dynamic circumstances. By minimizing the estimation error in the worst case, the H-infinity strategy can be used to address uncertainties in measurement noise [22]. However, it may break down in the presence of randomly occurring outliers [23]. The concept of M-estimation has been employed by UKF to resist the influences of measurement errors through the statistical linear regression of a nonlinear system function [24]. However, this method achieves the robustness by sacrificing the accuracy of the nonlinear system function itself [25]. By introducing scaling factors to inflate the covariance of measurement noise and further adjust the Kalman gain, the UKF performance can also be made robust against measurement errors [26]. However, since the scaling factors are determined empirically, this method may lead to a suboptimal filtering solution.

This paper presents a novel innovation orthogonality-based robust UKF (IO-RUKF) for tightly coupled INS/GNSS integration for hypersonic vehicle navigation. The IO-RUKF detects the errors in measurements through hypothesis testing. Based on this, it introduces a defined robust factor to inflate the covariance of predicted measurement and further decrease the Kalman gain such that the measurements in error are associated with a small weight to achieve the robustness against measurement errors. It should be noted that, different from the empirical determination of the scaling factors [26], the robust factor in the proposed IO-RUKF is derived based on the orthogonality of innovation vector in the framework of the derivative UKF and thus is optimal in theory. Simulations and comparison analysis have been conducted to comprehensively demonstrate the improved performance of the proposed IO-RUKF for hypersonic vehicle navigation.

II. TIGHTLY COUPLED INS/GNSS INTEGRATION

The basic principle of tightly coupled INS/GNSS integration is to use GNSS pseudorange data as the foundation measurements to estimate the navigation parameter error of INS through Kalman filtering. In this section, the mathematical model of tightly coupled INS/GNSS integration is established for the sake of INS error estimation.

A. PROCESS MODEL

In tightly coupled INS/GNSS integration, the INS error and GNSS receiver clock error are commonly chosen to form the system state vector. Thus, the process model is achieved by composing the error equations of the INS and GNSS receivers.

The navigation frame (n-frame) is selected as the E-N-U (East-North-Up) geography frame. Denote the inertial frame by i, the earth frame e, the body frame b and the INS simulated navigation frame n'. The error equations in terms of vehicle attitude and velocity can be formulated as [27], [28]

$$\begin{cases} \dot{\boldsymbol{\phi}} = -\hat{\boldsymbol{\omega}}_{in}^{n} \times \boldsymbol{\phi} + \delta\boldsymbol{\omega}_{in}^{n} - \boldsymbol{C}_{b}^{n'}\delta\boldsymbol{\omega}_{ib}^{b} \\ \delta\dot{\boldsymbol{v}}^{n} = \left(\boldsymbol{C}_{b}^{n'}\hat{\boldsymbol{f}}^{b}\right) \times \boldsymbol{\phi} + \boldsymbol{C}_{b}^{n'}\delta\boldsymbol{f}^{b} - (2\hat{\boldsymbol{\omega}}_{ie}^{n} + \hat{\boldsymbol{\omega}}_{en}^{n}) \\ \times\delta\boldsymbol{v}^{n} - (2\delta\boldsymbol{\omega}_{ie}^{n} + \delta\boldsymbol{\omega}_{en}^{n}) \times \hat{\boldsymbol{v}}^{n} \end{cases} \tag{1}$$

where $\boldsymbol{\phi} = (\phi_E, \phi_N, \phi_U)^T$ and $\delta\boldsymbol{v}^n = (\delta v_E, \delta v_N, \delta v_U)^T$ are the attitude error and velocity error in n-frame; $\hat{\boldsymbol{v}}^n = (\hat{v}_E, \hat{v}_N, \hat{v}_U)^T$ is the calculated velocity of the vehicle; $\boldsymbol{C}_b^{n'}$ are the rotation matrix from b frame to n' frame; $\hat{\boldsymbol{f}}^b$ is the measured specific force in the b-frame, whose error $\delta\boldsymbol{f}^b$ consists of the accelerometer zero-bias $\boldsymbol{\nabla}^b$ and white noise $\boldsymbol{\omega}_a^b$; $\delta\boldsymbol{\omega}_{ib}^b$ is the measurement error of the gyro, which is composed of constant drift $\boldsymbol{\varepsilon}^b$ and white noise $\boldsymbol{\omega}_g^b$; $\boldsymbol{\omega}_{ie}^n$ is the rotational

angular velocity of the earth; $\boldsymbol{\omega}_{en}^{n}$ is the angular velocity of the vehicle relative to the earth; $\boldsymbol{\omega}_{in}^{n} = \boldsymbol{\omega}_{ie}^{n} + \boldsymbol{\omega}_{en}^{n}$ is the relative angular velocity between n-frame and i-frame; $\hat{\boldsymbol{\omega}}_{ie}^{n}$, $\hat{\boldsymbol{\omega}}_{en}^{n}$ and $\hat{\boldsymbol{\omega}}_{in}^{n}$ are the actual values of $\boldsymbol{\omega}_{ie}^{n}$, $\boldsymbol{\omega}_{en}^{n}$ $\boldsymbol{\omega}_{in}^{n}$ in the n'-frame, and $\delta\boldsymbol{\omega}_{ie}^{n}$, $\delta\boldsymbol{\omega}_{en}^{n}$ and $\delta\boldsymbol{\omega}_{in}^{n}$ represent the corresponding errors.

The position error equation of INS is given by [28]

$$\begin{cases} \delta\dot{L} = \dfrac{\delta v_N}{R_M + \hat{h}} - \delta h \dfrac{v_N}{(R_M + \hat{h})^2} \\ \delta\dot{\lambda} = \dfrac{\delta v_E \sec\hat{L}}{R_N + \hat{h}} + \delta L \dfrac{v_E \tan\hat{L} \sec\hat{L}}{R_N + \hat{h}} - \delta h \dfrac{v_E \sec\hat{L}}{(R_N + \hat{h})^2} \\ \delta\dot{h} = \delta v_U \end{cases} \tag{2}$$

where $\delta\boldsymbol{p} = (\delta L, \delta\lambda, \delta h)$ is the position error in n-frame; $\hat{L}$ and $\hat{h}$ represent the latitude and altitude of the vehicle; and R_M and R_N are the median radius and normal radius.

Generally, the gyro constant drift $\boldsymbol{\varepsilon}^{b}$ and accelerometer zero-bias $\boldsymbol{\nabla}^{b}$ can be described by random constants [6], [18], i.e.

$$\dot{\boldsymbol{\varepsilon}}_i^b = 0 (i = x, y, z) \tag{3}$$

$$\dot{\boldsymbol{\nabla}}_i^b = 0 (i = x, y, z) \tag{4}$$

Define the system state of INS as

$$\boldsymbol{x}_{INS}(t) = [\boldsymbol{\phi}, \delta\boldsymbol{v}^n, \delta\boldsymbol{p}, \boldsymbol{\varepsilon}^b, \boldsymbol{\nabla}^b]^{\mathrm{T}} \tag{5}$$

The INS error equation can be obtained by combining (1)∼(4) according to the defined system state, that is

$$\dot{\boldsymbol{x}}_{INS}(t) = \mathbf{F}_{INS}(t)\boldsymbol{x}_{INS}(t) + \boldsymbol{w}_{INS}(t) \tag{6}$$

where $\boldsymbol{F}_{INS}(t)$ is the system dynamic matrix, and $\boldsymbol{w}_{INS}(t) = \left[\left(-\boldsymbol{C}_b^{n'}\boldsymbol{\omega}_a^b\right)^T, \left(\boldsymbol{C}_b^{n'}\boldsymbol{\omega}_g^b\right)^T, \mathbf{0}_{1\times 9}\right]^T$ is the noise vector.

The GNSS receiver clock usually introduces a time error which is translated into a range error. The error equation of the GNSS receiver can be modeled by [9]

$$\dot{\boldsymbol{x}}_{GNSS}(t) = \mathbf{F}_{GNSS}(t)\boldsymbol{x}_{GNSS}(t) + \boldsymbol{w}_{GNSS}(t) \tag{7}$$

where $\boldsymbol{x}_{GNSS}(t) = \left[b_p, b_f\right]^T$, b_p and b_f are the range bias and range drift related to the receiver clock, $\mathbf{F}_{GNSS}(t) = \begin{bmatrix} 0 & 1 \\ 0 & 0 \end{bmatrix}$ is the transition matrix and $\boldsymbol{w}_{GNSS}(t) = \left[w_p, w_f\right]^T$ is the noise vector.

Consequently, augmenting (7) into (6), the process model of tightly coupled INS/GPS integration can be obtained as:

$$\begin{bmatrix} \dot{\boldsymbol{x}}_{INS}(t) \\ \dot{\boldsymbol{x}}_{GNSS}(t) \end{bmatrix} = \begin{bmatrix} \mathbf{F}_{INS}(t) & 0 \\ 0 & \mathbf{F}_{GNSS}(t) \end{bmatrix} \begin{bmatrix} \boldsymbol{x}_{INS}(t) \\ \boldsymbol{x}_{GNSS}(t) \end{bmatrix} + \begin{bmatrix} \boldsymbol{w}_{INS}(t) \\ \boldsymbol{w}_{GNSS}(t) \end{bmatrix}$$

or

$$\dot{\boldsymbol{x}}(t) = \mathbf{F}(t)\boldsymbol{x}(t) + \boldsymbol{w}(t) \tag{8}$$

B. MEASUREMENT MODEL

The measurement model considered herein is based on the e-frame since the satellite position and velocity computed from the broadcast ephemeris parameters are given in this coordinate. For tightly coupled INS/GNSS integration, the standard measurement is the pseudorange which defines an approximate range from the GNSS receiver to a particular satellite. The pseudorange measurement from a GNSS receiver can be represented by

$$\rho^{(i)} = R^{(i)} + b_p + v^{(i)} \quad (i = 1, 2, ..., m) \tag{9}$$

where $R^{(i)} = ||\boldsymbol{r} - \boldsymbol{r}_s^{(i)}||$ is the geometric range from the ith satellite to the receiver, $\boldsymbol{r}$ the actual vehicle position vector, $\boldsymbol{r}_s^{(i)}$ the position vector of the ith satellite, b_p the range bias associated with the receiver clock, $v^{(i)}$ the measurement error modeled as white noise and m the number of observable satellites. Normally, it is assumed that the measurements from each satellite are independent of each other.

Suppose (x, y, z) is the actual vehicle position and (x_{si}, y_{si}, z_{si}) the ith satellite position in the e-frame. The geometric range $R^{(i)}$ in (9) can be expressed as

$$R^{(i)} = \sqrt{(x - x_{si})^2 + (y - y_{si})^2 + (z - z_{si})^2} \quad (i = 1, 2, ..., m) \tag{10}$$

It is verified that the coordinates of a vehicle's actual position in the e-frame and n-frame follow the relation

$$\begin{cases} x = (R_N + h)\cos L \cos\lambda \\ y = (R_N + h)\cos L \sin\lambda \\ z = \left[R_N\left(1 - f^2\right) + h\right]\sin L \end{cases} \tag{11}$$

where (x, y, z) is the position coordinate of the vehicle in the e-frame, (L, λ, h) the corresponding coordinate in the n-frame, R_N the radius of curvature in prime vertical and f the eccentricity of ellipsoid.

Denote the vehicle's position estimation obtained by INS as $\left(\hat{L}, \hat{\lambda}, \hat{h}\right)$. It is satisfied that

$$\begin{cases} \hat{L} = L + \delta L \\ \hat{\lambda} = \lambda + \delta\lambda \\ \hat{h} = h + \delta h \end{cases} \tag{12}$$

where $(\delta L, \delta\lambda, \delta h)$ is the position error in the state vector (9).

Then, by substituting (11) and (12) into (10), we can obtain

$$\begin{aligned} R^{(i)} = \Bigg\{ & \left[\left(R_N + (\hat{h} - \delta h)\right)\cos(\hat{L} - \delta L)\cos(\hat{\lambda} - \delta\lambda) - x_{si}\right]^2 \\ & + \left[\left(R_N + (\hat{h} - \delta h)\right)\cos(\hat{L} - \delta L)\sin(\hat{\lambda} - \delta\lambda) - y_{si}\right]^2 \\ & + \left[\left[R_N\left(1 - f^2\right) + (\hat{h} - \delta h)\right]\sin(\hat{L} - \delta L) - z_{si}\right]^2 \Bigg\}^{1/2} \end{aligned} \tag{13}$$

Subsequently, inserting (13) into (9), the measurement model for tightly coupled INS/GNSS integration is established. This model can be further rewritten as the standard

form of a nonlinear system, that is

$$\begin{aligned} z_k &= h(\delta L, \delta\lambda, \delta h) + v_k \\ &= h(\boldsymbol{x}_k) + v_k \end{aligned} \tag{14}$$

where $z_k = (\rho^{(1)}, \rho^{(2)}, \cdots, \rho^{(m)})^T$, $h(\cdot)$ is the nonlinear function describing the relationship between the pseudorange measurement and system state, and v_k is the measurement noise.

III. INNOVATION ORTHOGONALITY BASED ROBUST UKF

This section develops the IO-RUKF to restrain the impact of measurement errors for tightly coupled INS/GPS integration for hypersonic vehicle navigation. Since the process model (8) is linear while the measurement model (14) involves nonlinearity, the promising derivative version of UKF [9] which reduces the redundant computation in the prediction process, is adopted as the basis for establishment of the proposed IO-RUKF.

A. THE DERIVATIVE UKF

Considering the nonlinear discrete-time system with additive noises

$$\boldsymbol{x}_k = \mathbf{F}_{k/k-1}\boldsymbol{x}_{k-1} + \boldsymbol{w}_k \tag{15}$$

$$z_k = h(\boldsymbol{x}_k) + v_k \tag{16}$$

where $\mathbf{x}_k \in \mathbf{R}^n$ and $z_k \in \mathbf{R}^m$ denote the state and measurement vectors at time k; $\mathbf{F}_{k/k-1}$ is the discrete state transition matrix; $h(\cdot)$ is the nonlinear function describing the measurement model; and $\boldsymbol{w}_k \in \mathbf{R}^n$ and $v_k \in \mathbf{R}^m$ are the process and measurement noises, which are assumed as uncorrelated zero-mean Gaussian white noise processes with covariances

$$\mathrm{E}\left[\boldsymbol{w}_k \boldsymbol{w}_k^T\right] = \mathbf{Q}_k \text{ and } \mathrm{E}\left[v_k v_k^T\right] = \mathbf{R}_k \tag{17}$$

The procedure of the derivative UKF can be summarized as follows:

Step 1. Give the state estimate $\hat{\boldsymbol{x}}_{k-1}$ and the error covariance matrix $\hat{\mathbf{P}}_{k-1}$.

Step 2. Prediction: Since the process model is linear, the predicted state mean and covariance are performed with the same equations as the Kalman filter by

$$\hat{\boldsymbol{x}}_{k/k-1} = \mathbf{F}_{k/k-1}\hat{\boldsymbol{x}}_{k-1} \tag{18}$$

$$\hat{\mathbf{P}}_{k/k-1} = \mathbf{F}_{k/k-1}\hat{\mathbf{P}}_{k-1}\mathbf{F}_{k/k-1}^T + \mathbf{Q}_k \tag{19}$$

Step 3. Sigma Points Selection: A set of weighted sigma points are selected based on the predicted state mean and covariance. These sigma points are obtained by

$$\begin{cases} \boldsymbol{\xi}_{i,k/k-1} = \hat{\boldsymbol{x}}_{k/k-1} \\ \quad i = 0 \\ \boldsymbol{\xi}_{i,k/k-1} = \hat{\boldsymbol{x}}_{k/k-1} + a\left(\sqrt{n\hat{\mathbf{P}}_{k/k-1}}\right)_i \\ \quad i = 1, 2, \cdots, n \\ \boldsymbol{\xi}_{i,k/k-1} = \hat{\boldsymbol{x}}_{k/k-1} - a\left(\sqrt{n\hat{\mathbf{P}}_{k/k-1}}\right)_i \\ \quad i = n+1, n+2, \cdots, 2n \end{cases} \tag{20}$$

where $a \in \mathbf{R}$ is a tuning parameter to determine the spread of the sigma points around $\hat{\boldsymbol{x}}_{k/k-1}$ and is usually set as a small positive value. $\left(\sqrt{n\hat{\mathbf{P}}_{k/k-1}}\right)_i$ is the ith column of the matrix square root of $n\hat{\mathbf{P}}_{k/k-1}$.

Step 4. Update: The sigma points are instantiated through the nonlinear measurement model to yield a set of transformed samples

$$\boldsymbol{\gamma}_{i,k/k-1} = h(\boldsymbol{\xi}_{i,k/k-1}) \quad i = 0, 1, \cdots, 2n \tag{21}$$

The weighted mean and covariance of the predicted measurement are computed as

$$\hat{z}_{k/k-1} = \sum_{i=0}^{2n} \omega_i \boldsymbol{\gamma}_{i,k/k-1} \tag{22}$$

$$\hat{\mathbf{P}}_{\hat{z}_{k/k-1}} = \sum_{i=0}^{2n} \boldsymbol{\omega}_i \left(\boldsymbol{\gamma}_{i,k/k-1} - \hat{z}_{k/k-1}\right)\left(\boldsymbol{\gamma}_{i,k/k-1} - \hat{z}_{k/k-1}\right)^T + \mathbf{R}_k \tag{23}$$

and the cross-covariance between the predicted state and measurement is

$$\hat{\mathbf{P}}_{\hat{\boldsymbol{x}}_{k/k-1}\hat{z}_{k/k-1}} = \sum_{i=0}^{2n} \omega_i \left(\boldsymbol{\xi}_{i,k/k-1} - \hat{\boldsymbol{x}}_{k/k-1}\right) \times \left(\boldsymbol{\gamma}_{i,k/k-1} - \hat{z}_{k/k-1}\right)^T \tag{24}$$

where $\begin{cases} \omega_i = 1 - \frac{1}{a^2} & i = 0 \\ \omega_i = \frac{1}{2na^2} & i = 1, 2, \cdots, 2n \end{cases}$

The Kalman gain is determined by

$$\mathbf{K}_k = \hat{\mathbf{P}}_{\hat{\boldsymbol{x}}_{k/k-1}\hat{z}_{k/k-1}}\hat{\mathbf{P}}_{\hat{z}_{k/k-1}}^{-1} \tag{25}$$

Then, the state $\hat{\boldsymbol{x}}_k$ and the corresponding error covariance matrix $\hat{\boldsymbol{P}}_k$ can be updated as

$$\hat{\boldsymbol{x}}_k = \hat{\boldsymbol{x}}_{k/k-1} + \mathbf{K}_k(z_k - \hat{z}_{k/k-1}) \tag{26}$$

$$\hat{\mathbf{P}}_k = \hat{\mathbf{P}}_{k/k-1} - \mathbf{K}_k\hat{\mathbf{P}}_{\hat{z}_{k/k-1}}\mathbf{K}_k^T \tag{27}$$

Step 5. Repeat steps 1 to 4 for the next sample.

B. THE PROPOSED IO-RUKF

The core concept of the proposed IO-RUKF is to introduce a time-varying robust factor into the covariance of predicted measurement to rescale the Kalman gain such that the contribution of contaminated measurements on state estimation can be less weighted to achieve the robustness against measurement errors. A modified covariance of the predicted measurement is defined as

$$\hat{\mathbf{P}}_{\hat{z}_{k/k-1}}^* = s_k\hat{\mathbf{P}}_{\hat{z}_{k/k-1}} \tag{28}$$

where s_k is the robust factor.

If no measurement error is existed, the robust factor is $s_k = 1$, which signifies that the proposed IO-RUKF is carried out according to the derivative UKF as described by (18)~(27). Otherwise, a robust factor greater than 1 is

incorporated in the filtering process to inflate the covariance of predicted measurement as in (28).

Define the innovation vector of UKF by

$$\tilde{z}_k = z_k - \hat{z}_{k/k-1} \tag{29}$$

It is well known that as the system models (15) and (16) are accurate, the output innovation sequence $\tilde{z}_k (k = 1, 2, \cdots, N)$ should be Gaussian distributed with zero mean and satisfy the orthogonality principle [29], that is

$$\mathrm{E}\left[\tilde{z}_k^T \cdot \tilde{z}_{k+j}\right] = \mathbf{0} \quad (j = 1, 2, \cdots) \tag{30}$$

Nevertheless, in case of measurement errors (such as outliers in pseudorange observations and non-Gaussian noise distribution), the violation of the assumption in (15) and (16) may result in biased or unstable state estimation from UKF, and further make (30) no longer hold. For this case, we determine the robust factor by compelling the innovation sequence to be orthogonal to each other, so that the useful information in the innovation sequence is extracted and the UKF filtering process is corrected by adjusting the Kalman gain.

Denote the estimation error and prediction error by

$$\tilde{\boldsymbol{x}}_k = \boldsymbol{x}_k - \hat{\boldsymbol{x}}_k \tag{31}$$

$$\tilde{\boldsymbol{x}}_{k/k-1} = \boldsymbol{x}_k - \hat{\boldsymbol{x}}_{k/k-1} \tag{32}$$

Inserting (15) and (18) into (32), it is obtained that

$$\begin{aligned}\tilde{\boldsymbol{x}}_{k/k-1} &= \mathbf{F}_k\left(\boldsymbol{x}_{k-1} - \hat{\boldsymbol{x}}_{k-1}\right) + \boldsymbol{w}_k \\ &= \mathbf{F}_k\tilde{\boldsymbol{x}}_{k-1} + \boldsymbol{w}_k\end{aligned} \tag{33}$$

Expanding $\boldsymbol{z}_k$ by the Taylor series about $\hat{\boldsymbol{x}}_{k/k-1}$, we have

$$\begin{aligned}\boldsymbol{z}_k = {} & h(\hat{\boldsymbol{x}}_{k/k-1}) + \nabla h(\hat{\boldsymbol{x}}_{k/k-1})\tilde{\boldsymbol{x}}_{k/k-1} \\ & + \nabla^2 h(\hat{\boldsymbol{x}}_{k/k-1})\tilde{\boldsymbol{x}}_{k/k-1}^2 + \cdots + \boldsymbol{v}_k\end{aligned} \tag{34}$$

where the ith term in the Taylor series for $h(\cdot)$ is $\nabla^i h(\hat{\boldsymbol{x}}_{k/k-1})\tilde{\boldsymbol{x}}_{k/k-1}^i = \frac{1}{i!}\left(\sum_{j=1}^{n}\tilde{x}_j\frac{\partial}{\partial x_j}\right)^i h(\boldsymbol{x})\Big|_{\boldsymbol{x}=\hat{\boldsymbol{x}}_{k/k-1}}$; and x_j denotes the jth component of $\boldsymbol{x}$.

Similarly, expanding $\hat{z}_{k/k-1}$ given in (22) by the Taylor series yields

$$\begin{aligned}\hat{\boldsymbol{z}}_{k/k-1} = {} & \left(1 - \frac{1}{a^2}\right)h(\hat{\boldsymbol{x}}_{k/k-1}) + \frac{1}{2na^2}\sum_{i=1}^{n} \\ & \times h\left[\hat{\boldsymbol{x}}_{k/k-1} + a\left(\sqrt{n\hat{\mathbf{P}}_{k/k-1}}\right)_i\right] \\ & + \frac{1}{2na^2}\sum_{i=n+1}^{2n} h\left[\hat{\boldsymbol{x}}_{k/k-1} - a\left(\sqrt{n\hat{\mathbf{P}}_{k/k-1}}\right)_{i-n}\right] \\ = {} & h(\hat{\boldsymbol{x}}_{k/k-1}) + \frac{1}{2}\nabla^2 h(\hat{\boldsymbol{x}}_{k/k-1})\hat{\mathbf{P}}_{k/k-1} + \cdots\end{aligned} \tag{35}$$

Substituting (34) and (35) into (29), the innovation vector $\tilde{\boldsymbol{z}}_k$ can be rewritten as

$$\tilde{\boldsymbol{z}}_k = \mathbf{H}_k\tilde{\boldsymbol{x}}_{k/k-1} + \Delta(\tilde{\boldsymbol{x}}_{k/k-1}) + \boldsymbol{v}_k \tag{36}$$

where $\mathbf{H}_k = \frac{\partial h(\boldsymbol{x})}{\partial \boldsymbol{x}}\Big|_{\boldsymbol{x}=\hat{\boldsymbol{x}}_{k/k-1}}$, and $\Delta(\tilde{\boldsymbol{x}}_{k/k-1})$ denotes the second- and higher-order moments in the Taylor series.

To simplify the error expression, the unknown instrumental diagonal matrices $\boldsymbol{\alpha}_k = diag(\alpha_{1,k}, \alpha_{2,k}, \cdots, \alpha_{m,k})$ are employed to model the errors due to the first-order linearization [30], leading to the following exact equality

$$\tilde{\boldsymbol{z}}_k = \boldsymbol{\alpha}_k\mathbf{H}_k\tilde{\boldsymbol{x}}_{k/k-1} + \boldsymbol{v}_k \tag{37}$$

Substituting (33) into (37), it is also evident that

$$\tilde{\boldsymbol{z}}_k = \boldsymbol{\alpha}_k\mathbf{H}_k\left(\mathbf{F}_k\tilde{\boldsymbol{x}}_{k-1} + \boldsymbol{w}_k\right) + \boldsymbol{v}_k \tag{38}$$

Subsequently, we denote $\mathbf{Y}_{j,k} = \mathrm{E}\left[\tilde{\boldsymbol{z}}_{k+j} \cdot \tilde{\boldsymbol{z}}_k^T\right]$. From the presentation of $\tilde{\boldsymbol{z}}_k$ in (29) and (38), $\mathbf{Y}_{j,k}$ can be rewritten as

$$\begin{aligned}\mathbf{Y}_{j,k} = \mathrm{E}\Big\{ & \left[\boldsymbol{\alpha}_{k+j}\mathbf{H}_{k+j}\left(\mathbf{F}_{k+j}\tilde{\boldsymbol{x}}_{k+j-1} + \boldsymbol{w}_{k+j}\right) + \boldsymbol{v}_{k+j}\right] \\ & \cdot(\boldsymbol{z}_k - \hat{\boldsymbol{z}}_{k/k-1})^T\Big\}\end{aligned} \tag{39}$$

Then, by substituting (31), (26) and (38) into (39) and applying the result of (33) recursively, (39) can be furtherly derived as (40), as shown at the bottom of this page, where the properties of the Gaussian white noise processes, i.e. $\mathrm{E}\left[\boldsymbol{w}_i\boldsymbol{w}_j^T\right] = \mathbf{0}$, $\mathrm{E}\left[\boldsymbol{v}_i\boldsymbol{v}_j^T\right] = \mathbf{0}$ $(i \neq j)$ and $\mathrm{E}\left[\boldsymbol{w}_i\boldsymbol{v}_j^T\right] = \mathbf{0}$

$$\begin{aligned}\boldsymbol{Y}_{j,k} &= \mathrm{E}\left\{\left[\boldsymbol{\alpha}_{k+j}\mathbf{H}_{k+j}\mathbf{F}_{k+j}\left(\boldsymbol{x}_{k+j-1} - \hat{\boldsymbol{x}}_{k+j-1/k+j-2} - \mathbf{K}_{k+j-1}(\boldsymbol{z}_{k+j-1} - \hat{\boldsymbol{z}}_{k+j-1/k+j-2})\right)\right] \cdot (\boldsymbol{z}_k - \hat{\boldsymbol{z}}_{k/k-1})^T\right\} \\ &= \mathrm{E}\left\{\left[\boldsymbol{\alpha}_{k+j}\boldsymbol{H}_{k+j}\mathbf{F}_{k+j}\left(\mathbf{F}_{k+j-1}\tilde{\boldsymbol{x}}_{k+j-2} - \mathbf{K}_{k+j-1}\left(\boldsymbol{\alpha}_{k+j-1}\mathbf{H}_{k+j-1}\mathbf{F}_{k+j-1}\tilde{\boldsymbol{x}}_{k+j-2}\right)\right)\right] \cdot (\boldsymbol{z}_k - \hat{\boldsymbol{z}}_{k/k-1})^T\right\} \\ &= \mathrm{E}\left\{\left[\boldsymbol{\alpha}_{k+j}\mathbf{H}_{k+j}\mathbf{F}_{k+j}\left(\mathbf{I} - \mathbf{K}_{k+j-1}\boldsymbol{\alpha}_{k+j-1}\mathbf{H}_{k+j-1}\right)\mathbf{F}_{k+j-1}\tilde{\boldsymbol{x}}_{k+j-2}\right] \cdot (\boldsymbol{z}_k - \hat{\boldsymbol{z}}_{k/k-1})^T\right\} \\ &= \boldsymbol{\alpha}_{k+j}\mathbf{H}_{k+j}\mathbf{F}_{k+j} \cdot \left(\prod_{i=k+1}^{k+j-1}(\mathbf{I} - \mathbf{K}_i\boldsymbol{\alpha}_i\mathbf{H}_i)\mathbf{F}_i\right) \cdot \mathrm{E}\left\{\left[\boldsymbol{x}_k - \hat{\boldsymbol{x}}_{k/k-1} - \mathbf{K}_k(\boldsymbol{z}_k - \hat{\boldsymbol{z}}_{k/k-1})\right] \cdot (\boldsymbol{z}_k - \hat{\boldsymbol{z}}_{k/k-1})^T\right\} \\ &= \boldsymbol{\alpha}_{k+j}\mathbf{H}_{k+j}\mathbf{F}_{k+j} \cdot \left(\prod_{i=k+1}^{k+j-1}(\mathbf{I} - \mathbf{K}_i\boldsymbol{\alpha}_i\mathbf{H}_i)\mathbf{F}_i\right) \cdot \left(\hat{\mathbf{P}}_{\hat{\boldsymbol{x}}_{k/k-1}\hat{\boldsymbol{z}}_{k/k-1}} - \mathbf{K}_k\mathbf{Y}_{0,k}\right)\end{aligned} \tag{40}$$

are used, and $\boldsymbol{Y}_{0,k}$ is the actual innovation covariance output by UKF which is calculated as [16]

$$\mathbf{Y}_{0,k} = \begin{cases} \tilde{z}_1 \tilde{z}_1^T, & k = 1 \\ \dfrac{\rho \cdot \mathbf{Y}_{0,k-1} + \tilde{z}_k \tilde{z}_k^T}{1+\rho}, & k > 1 \end{cases} \tag{41}$$

where $0 < \rho \leq 1$ is a forgetting factor and is generally set as $\rho = 0.95$.

For determining the robust factor analytically, the modified covariance of predicted measurement (28) is considered to compel the innovation sequence to be orthogonal. Let $\mathbf{Y}_{j,k} = 0$, it can be deduced from (40) that

$$\mathbf{K}_k \cdot \left(\hat{\mathbf{P}}^*_{\hat{z}_{k/k-1}} - \mathbf{Y}_{0,k} \right) = \mathbf{0} \tag{42}$$

which is equivalent to

$$s_k \hat{\mathbf{P}}_{\hat{z}_{k/k-1}} = \mathbf{Y}_{0,k} \tag{43}$$

Thus, by taking the trace of both sides of (43), we obtain the robust factor

$$s_k = \frac{tr\left(\mathbf{Y}_{0,k}\right)}{tr\left(\hat{\mathbf{P}}_{\hat{z}_{k/k-1}}\right)} \tag{44}$$

Noticing that in the presence of measurement errors, the innovation vector $\tilde{z}_k$ will be biased and its magnitude will increase. As a result, the trace of the innovation covariance $\mathbf{Y}_{0,k}$ output from UKF becomes larger than that of the predicted measurement covariance $\hat{\mathbf{P}}_{\hat{z}_{k/k-1}}$. It is easy to verify that the robust factor obtained by (44) is generally greater than 1, which makes up a decrement in the Kalman gain as shown in (25) and (28). Therefore, the measurements in error are associated with a small weight in the estimation process to inhibit the disturbances of measurement errors on the state estimation.

Actually, the measurement errors can be detected via the statistical information of the innovation sequence using hypothesis test. Define the statistical function

$$\theta_k = \tilde{z}_k^T \cdot \mathbf{P}^{-1}_{\hat{z}_{k/k-1}} \cdot \tilde{z}_k \tag{45}$$

and the following two hypotheses:

Null hypothesis γ_0: the system is normally operating;

Alternative hypothesis γ_1: there exist measurement errors in the estimation system.

The statistical function θ_k obeys a χ^2 distribution with m degree of freedom. For a chosen significance level $\alpha(0 < \alpha \leq 1)$, from

$$P(\chi^2 > \chi^2_{\alpha,m}) = \alpha \tag{46}$$

a threshold value $\chi^2_{\alpha,m}$ can be determined and the statistical function θ_k will be greater than the threshold value $\chi^2_{\alpha,m}$ if the alternative hypothesis is correct, that is

$$\begin{aligned} &\gamma_0 : \theta_k \leq \chi^2_{\alpha,m} \quad \forall k \\ &\gamma_1 : \theta_k > \chi^2_{\alpha,m} \quad \exists k \end{aligned} \tag{47}$$

Consequently, based on the above derivations, the flow chart of the proposed IO-RUKF is depicted in Fig. 1. It can be seen that the procedure for implementing the IO-RUKF involves the following main steps:

Step 1. Initiate the filter with the state estimate $\hat{\boldsymbol{x}}_{k-1}$ and the error covariance matrix $\hat{\mathbf{P}}_{k-1}$;

Step 2. Execute the derivative UKF from (18) to (23);

Step 3. Calculate the innovation vector through (29) and detect the measurement errors using the hypothesis test described by (45)-(47);

If a measurement error is detected, do the following two operations:

- Compute the robust factor through (44) and replace $\hat{\mathbf{P}}_{\hat{z}_{k/k-1}}$ with its modified type $\hat{\mathbf{P}}^*_{\hat{z}_{k/k-1}} = s_k \hat{\mathbf{P}}_{\hat{z}_{k/k-1}}$ as presented in (28).
- Then complete the update procedure as (24)-(27).

Otherwise, complete the derivative UKF procedure directly as (24)-(27).

Step 4. Repeat Steps 1 to 3 for the next time step.

Remark 1: In addition to (28), the inflation of the covariance of predicted measurement can also be conducted in the following two different forms:

$$\hat{\mathbf{P}}^*_{\hat{z}_{k/k-1}} = s_k \cdot \sum_{i=0}^{2n} \omega_i \left(\boldsymbol{\gamma}_{i,k/k-1} - \hat{z}_{k/k-1} \right) \times \left(\boldsymbol{\gamma}_{i,k/k-1} - \hat{z}_{k/k-1} \right)^{\boldsymbol{T}} + \mathbf{R}_k \tag{48}$$

and

$$\hat{\mathbf{P}}^*_{\hat{z}_{k/k-1}} = \sum_{i=0}^{2n} \omega_i \left(\boldsymbol{\gamma}_{i,k/k-1} - \hat{z}_{k/k-1} \right) \times \left(\boldsymbol{\gamma}_{i,k/k-1} - \hat{z}_{k/k-1} \right)^{\boldsymbol{T}} + s_k \cdot \mathbf{R}_k \tag{49}$$

Although (28), (48) and (49) provides different ways to calculate the robust factor, they play a similar role in rescaling the Kalman gain and enhancing the UKF robustness against measurement errors.

Remark 2: Different from the empirical determination of the scaling factors [26], the robust factor in the proposed IO-RUKF is obtained based on the innovation orthogonality in the framework of the derivative UKF. Therefore, the robust factor of the proposed IO-RUKF is of optimality in theory.

Remark 3: From (23) and (28), we represent the modified covariance of predicted measurement as

$$\hat{\mathbf{P}}^*_{\hat{z}_{k/k-1}} = \hat{\mathbf{P}}_{\hat{z}_{k/k-1}} + (s_k - 1)\, \hat{\mathbf{P}}_{\hat{z}_{k/k-1}} \tag{50}$$

Since $s_k \geq 1$, $(s_k - 1)\, \hat{\mathbf{P}}_{\hat{z}_{k/k-1}}$ is a nonnegative definite matrix. In addition to the instrumental diagonal matrix $\boldsymbol{\alpha}_k$ introduced in (37), similar to our previous work [31], an instrumental matrix $\boldsymbol{\gamma}_k \in \mathbf{R}^{m \times m}$ can also be used to describe the approximation error for calculating $\hat{\mathbf{P}}_{\hat{\boldsymbol{x}}_{k/k-1}\hat{z}_{k/k-1}}$. Thus (50) can be rewritten as

$$\begin{aligned} \hat{\mathbf{P}}^*_{\hat{z}_{k/k-1}} &= \boldsymbol{\gamma}_k^T \boldsymbol{\alpha}_k \mathbf{H}_k \hat{\mathbf{P}}_{k/k-1} \mathbf{H}_k^T \boldsymbol{\alpha}_k \boldsymbol{\gamma}_k + \mathbf{R}^*_k + (s_k - 1)\, \hat{\mathbf{P}}_{\hat{z}_{k/k-1}} \\ &= \boldsymbol{\gamma}_k^T \boldsymbol{\alpha}_k \mathbf{H}_k \hat{\mathbf{P}}_{k/k-1} \mathbf{H}_k^T \boldsymbol{\alpha}_k \boldsymbol{\gamma}_k + \mathbf{R}^{**}_k \end{aligned} \tag{51}$$

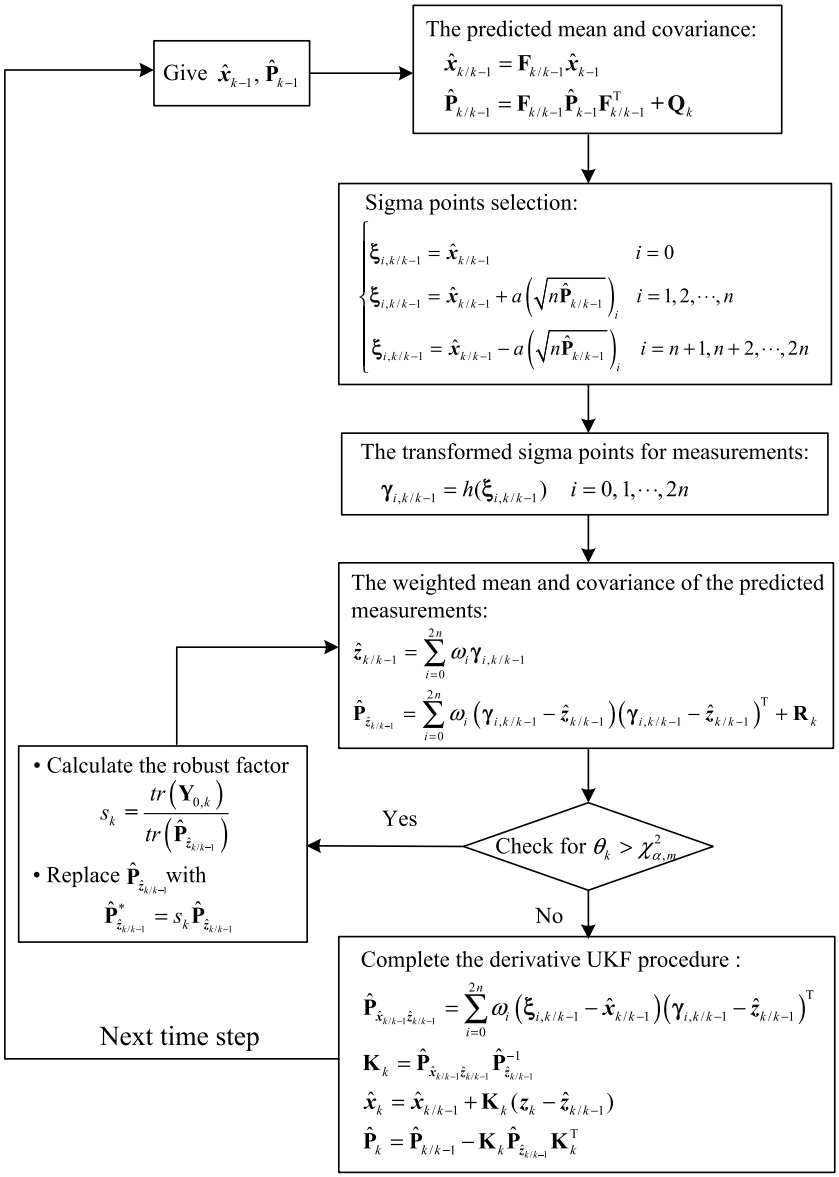

FIGURE 1. Flow chart of the proposed IO-RUKF.

where $\mathbf{R}_k^{**} = \mathbf{R}_k^{*} + (s_k - 1)\hat{\mathbf{P}}_{\hat{z}_{k/k-1}}$; and $\mathbf{R}_k^{*}$ is the equivalent measurement noise covariance defined by equation (25) in [31].

Accordingly, the sufficient conditions to guarantee the stochastic stability of the proposed IO-RUKF can be easily obtained by applying the result of ***Theorem 1*** reported in [31]. The details are presented as follows.

Consider the nonlinear stochastic systems given by (15), and (16) as well as the IO-RUKF derived in Part B, Section III. Let the following conditions hold for every $k \geq 0$:

(i) There exist real constants $f_{\min}$, $f_{\max}$, $c_{\min}$, $c_{\max}$, $h_{\min}$, $h_{\max}$, $\eta_{\max}$, $\kappa_{\max} > 0$ such that the following bounds are fulfilled:

$$f_{\min} \leq \left\|\mathbf{F}_{k/k-1}\right\| \leq f_{\max} \tag{52}$$

$$c_{\min} \leq \left\|\boldsymbol{\gamma}_k^{T}\boldsymbol{\alpha}_k\mathbf{H}_k\right\| \leq c_{\max} \tag{53}$$

$$h_{\min} \leq \left\|\boldsymbol{\alpha}_k\mathbf{H}_k\right\| \leq h_{\max} \tag{54}$$

$$\max_{i,j=1,2,\cdots,n}\left[\left|\left(\mathbf{H}_k^{T}\alpha_k\boldsymbol{\gamma}_k\right)_{i,j}\right|\right] \leq \eta_{\max} \tag{55}$$

$$\max_{i,j=1,2,\cdots,n}\left[\left|\left(\boldsymbol{\alpha}_k\mathbf{H}_k\right)_{i,j}\right|\right] \leq \kappa_{\max} \tag{56}$$

where $h_{\min} \leq c_{\max}$.

(ii) There exist real constants $r^{*}_{\min}$, $r^{*}_{\max}$, $r_{\max}$, $q_{\min}$, $q_{\max}$, $p_{\min}$, $p_{\max} > 0$ such that the following bounds on various matrices are fulfilled:

$$r^{*}_{\min}\mathbf{I} \leq \mathbf{R}_k^{*} \leq r^{*}_{\max}\mathbf{I} \tag{57}$$

$$\mathbf{R}_k \leq r_{\max}\mathbf{I} \tag{58}$$

$$p_{\min}\mathbf{I} \leq \hat{\mathbf{P}}_k \leq p_{\max}\mathbf{I} \tag{59}$$

$$q_{\min}\mathbf{I} \leq \mathbf{Q}_k \leq q_{\max}\mathbf{I} \tag{60}$$

(iii) There exists a real constant $\varepsilon_{\max} > 0$ such that the following matrix norm is bounded via

$$\left\| \boldsymbol{\gamma}_k^T \boldsymbol{\alpha}_k \mathrm{H}_k - \boldsymbol{\alpha}_k \mathbf{H}_k \right\| \leq \varepsilon_{\max} \tag{61}$$

where $\varepsilon_{\max}^2 \leq \frac{r_{\min}^*}{\phi_{\max}^2 (p_{\max} + p_{\max}^2 \phi_{\max}^2 / q_{\min})}$, and $\|\cdot\|$ denotes the Euclidian norm.

Then stochastic stability of the IO-RUKF is ensured, i.e, the estimation error $\tilde{\boldsymbol{x}}_k$ of the IO-RUKF is exponentially bounded in mean square.

IV. SIMULATIONS AND RESULTS

Simulations were conducted to comprehensively evaluate the performance of the proposed IO-RUKF for tightly coupled INS/GNSS integration in hypersonic vehicle navigation. The typical measurement errors, i.e. outliers in pseudorange observations and non-Gaussian noise distribution caused by hypersonic vehicle's high maneuverability, are considered. The comparison of the proposed IO-RUKF with the derivative UKF (DUKF) and robust UKF (RUKF) in [26] is also discussed.

Fig. 2 depicts the dynamic flight trajectory of a hypersonic vehicle, which was designed to involve various flight maneuvers such as climbing, pitching, rolling and turning. The simulation parameters are shown in Table 1. The simulation time was 1000s and the filtering period was 0.1s. To detect the measurement error, $\chi_{\alpha,m}^2$ in the proposed IO-RUKF was set as 9.488 which was acquired from the χ^2 distribution under 4 degrees of freedom ($m = 4$) and 95% confidence level ($\alpha = 0.05$). The simulation trials were conducted for the two typical measurement errors, i.e. outliers in pseudorange observations and the non-Gaussian distribution of measurement noise.

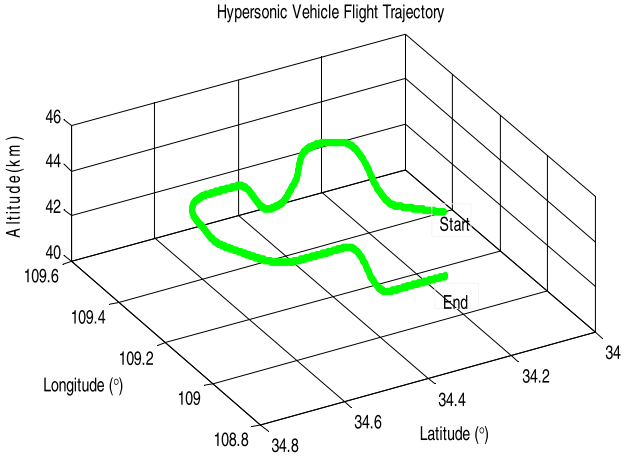

FIGURE 2. Flight trajectory of a hypersonic vehicle.

Through the simulation analysis, the overall estimation error and its corresponding mean squared error (MSE) for Monte Carlo runs were adopted to evaluate the navigation accuracy for DUKF, RUKF and IO-RUKF. The overall estimation error is defined as the norm of the navigation

TABLE 1. Simulation parameters.

Initial position	East longitude	109.4°
	North latitude	34.025°
	Altitude	40km
Initial velocity	East	1500 m/s
	North	1700 m/s
	Up	0 m/s
Initial attitude	Pitch	0
	Roll	0
	Yaw	0
Initial position error	East longitude	15m
	North latitude	15m
	Altitude	20m
Initial velocity error	East	0.5 m/s
	North	0.5 m/s
	Up	0.5 m/s
Initial attitude error	Pitch	1′
	Roll	1′
	Yaw	1.5′
Gyro parameters	Constant drift	0.05° / h
	White noise	0.01° / h
	Sampling frequency	50Hz
Accelerometer parameters	Zero bias	$10^{-3}\,g$
	White noise	$10^{-4}\,g$
	Sampling frequency	50Hz
GNSS parameters	Pseudorange measurement error	25m
	Sampling frequency	10Hz

parameters estimation error

$$\left\| \Delta\hat{x} \right\| = \sqrt{\Delta\hat{x}_E^2 + \Delta\hat{x}_N^2 + \Delta\hat{x}_U^2} \tag{62}$$

where $\Delta\hat{x}_E$, $\Delta\hat{x}_N$ and $\Delta\hat{x}_U$ are the components of $\Delta\hat{x}$ in East, North and Up, respectively. The MSE of the overall estimation error for each Monte Carlo run is defined by

$$MSE(m_S) = \frac{1}{T} \sum_{k=1}^{T} \left(\left\| \Delta\hat{x}(k) \right\| \right)^2 \quad (m_S = 1, \cdots, M) \tag{63}$$

where T is the time steps involved in the filtering process and M is the number of Monte Carlo runs.

A. OUTLIERS IN PSEUDORANGE OBSERVATIONS

To evaluate the performance of the proposed IO-RUKF in terms of outliers in pseudorange observations, a pseudorange observation error of 80m was artificially introduced into (10) every 200s.

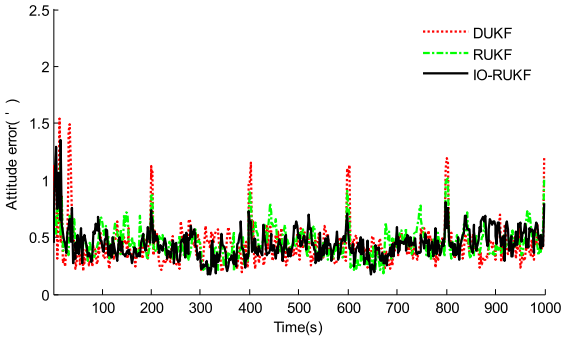

FIGURE 3. Attitude error of hypersonic vehicle for the case with observation outliers.

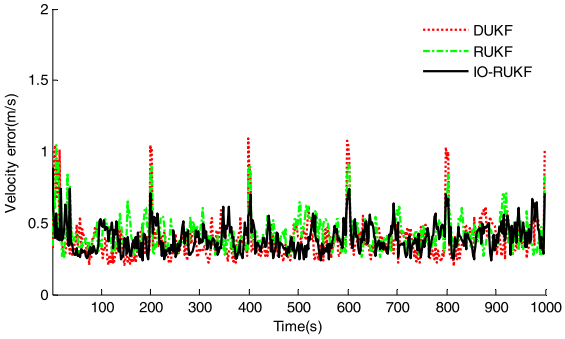

FIGURE 4. Velocity error of hypersonic vehicle for the case with observation outliers.

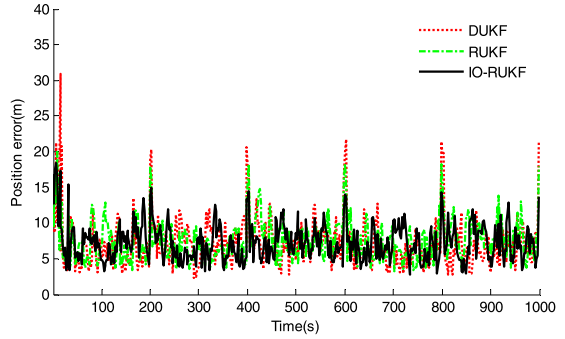

FIGURE 5. Position error of hypersonic vehicle for the case with observation outliers.

Figs. 3∼5 illustrate the overall attitude errors, velocity errors and position errors obtained by the DUKF, RUKF and IO-RUKF. When the observation outlier appears at the time points 200s, 400s, 600s, 800s and 1000s, the performance of DUKF degrades seriously due to the influence of outlier. RUKF improves DUKF by incorporating scaling factors in the measurement noise covariance to adjust the Kalman gain matrix, leading to the improved filtering result for navigation. However, because the scaling factors are determined by empiricism, RUKF still has pronounced estimation errors in the case of observation outlier. In contrast, since the proposed IO-RUKF determines the robust factor based on the innovation orthogonality principle, its resultant errors in attitude, velocity and position are the smallest. Furthermore, for the

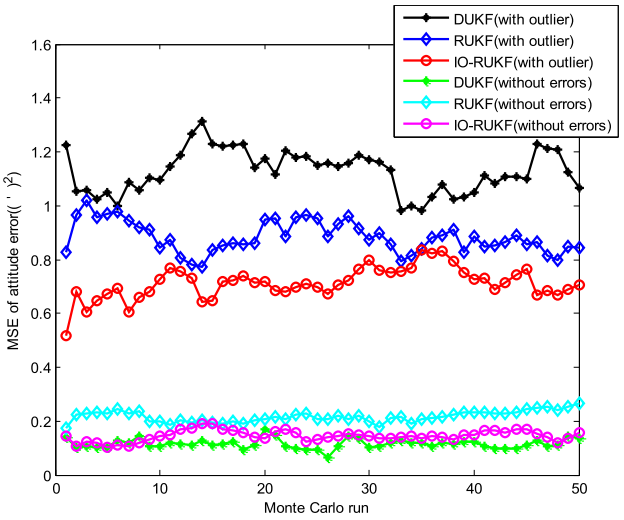

FIGURE 6. MSE of attitude error for the case with observation outliers.

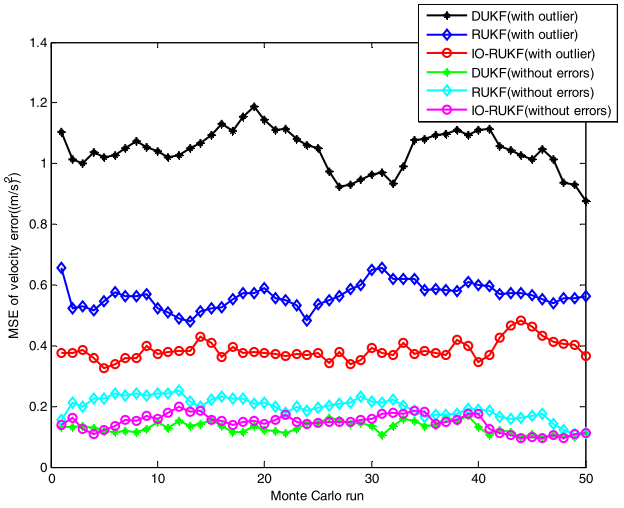

FIGURE 7. MSE of velocity error for the case with observation outliers.

time periods without the observation outlier, RUKF has poor navigation accuracy in comparison to DUKF and IO-RUKF. This is because RUKF does not involve the detection of observation outlier, that is, it still embeds the scaling factors in the filtering process even if the observation is accurate, thus deteriorating the filtering solution. The mean overall errors in attitude, velocity and position for the times with the outlier and the other time periods by the three filters are given in Table 2, which verifies the above phenomenon.

Besides, by repeating the above simulation for 50 runs, Monte Carlo method have also been employed to evaluate the IO-RUKF robustness from a statistical perspective. Figs. 6∼8 show the MSEs of attitude error, velocity error and position error achieved by the DUKF, RUKF and IO-RUKF. From Figs. 6∼8, the similar conclusion with the Figs. 3∼5 can be obtained. In the case of observation with outliers, the proposed IO-RUKF performs the best compared with DUKF and RUKF, since it has the capability to detect

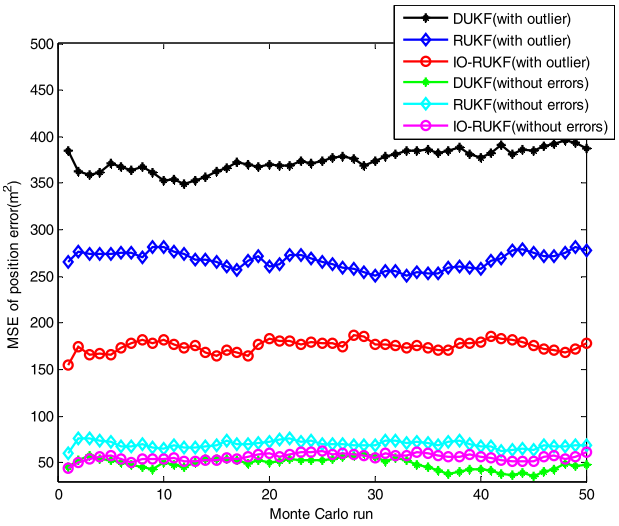

FIGURE 8. MSE of position error for the case with observation outliers.

TABLE 2. Mean overall navigation errors of hypersonic vehicle navigation for the case with observation outliers.

Filtering methods	Navigation errors	Mean errors	
		Times with outlier	Other time periods
DUKF	Attitude error (′)	1.1063	0.3737
	Velocity error (m/s)	1.0516	0.3637
	Position error (m)	19.6228	6.3476
RUKF	Attitude error (′)	0.9092	0.4152
	Velocity error (m/s)	0.8112	0.3944
	Position error (m)	16.3102	7.4397
IO-RUKF	Attitude error (′)	0.7191	0.3801
	Velocity error (m/s)	0.6134	0.3719
	Position error (m)	12.4676	6.2683

the outlier and adjust the Kalman gain matrix online to inhibit the undesirable influence of measurement error on the navigation accuracy. For the time without observation outlier, the DUKF outperforms the RUKF and IO-RUKF. This result is not surprising, because in this case the DUKF is optimal based on the minimum mean-square error sense. Nevertheless, it is notable that since the IO-RUKF involves the observation outlier detection process, the proposed method achieves preferable navigation accuracy comparing to RUKF.

B. NON-GAUSSIAN NOISE DISTRIBUTION

To evaluate the performance of the proposed IO-RUKF in terms of the non-Gaussian characteristics of noise statistics, the measurement noise is suddenly changed to a Gaussian mixture distribution in the following form for the time period (400s, 600s)

$$\boldsymbol{v}_k \sim (1-\mu)N(0, \mathbf{R}_k) + \mu N(0, 15 \cdot \mathbf{R}_k) \tag{64}$$

where μ is set to 0.3.

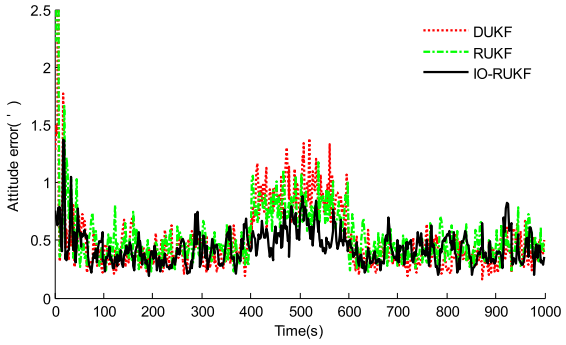

FIGURE 9. Attitude error of hypersonic vehicle navigation for the case with non-Gaussian measurement noise.

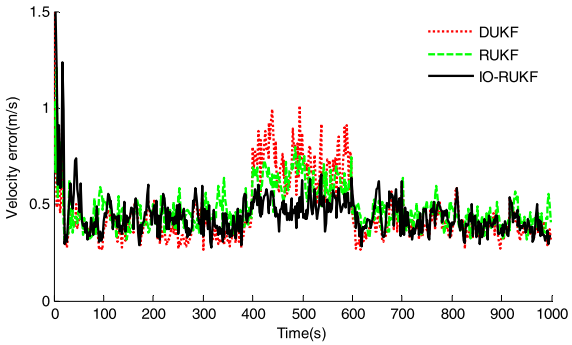

FIGURE 10. Velocity error of hypersonic vehicle navigation for the case with non-Gaussian measurement noise.

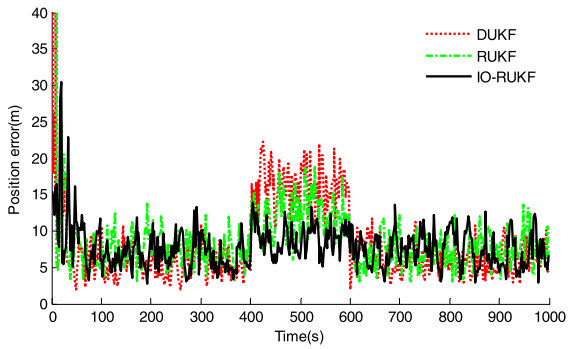

FIGURE 11. Position error of hypersonic vehicle navigation for the case with non-Gaussian measurement noise.

Figs. 9∼11 show the overall attitude errors, velocity errors and position errors obtained by the DUKF, RUKF and IO-RUKF for the case with non-Gaussian measurement noise. During the time interval (400s, 600s), due to the influence of the non-Gaussian measurement noise, DUKF has the poor navigation accuracy comparing to RUKF and IO-RUKF. This is because DUKF has no ability to inhibit the influence of the non-Gaussian noise distribution on the state estimation. The RUKF and IO-RUKF can resist the disturbance of the non-Gaussian measurement noise by introducing the scaling factors and robust factor to adjust the Kalman gain, respectively. Nevertheless, as expected, the navigation accuracy achieved by IO-RUKF is superior to that of RUKF. This is

TABLE 3. Mean overall navigation errors of hypersonic vehicle navigation for the case with non-Gaussian measurement noise.

Filtering methods	Navigation errors	Mean errors	
		(400s, 600s) with non-Gaussian noise	Other time periods
DUKF	Attitude error (′)	0.8842	0.3726
	Velocity error (m/s)	0.7181	0.3680
	Position error (m)	16.2703	6.1716
RUKF	Attitude error (′)	0.8169	0.4184
	Velocity error (m/s)	0.6208	0.4106
	Position error (m)	12.2637	7.5007
IO-RUKF	Attitude error (′)	0.5581	0.3681
	Velocity error (m/s)	0.4974	0.3835
	Position error (m)	9.0467	6.3035

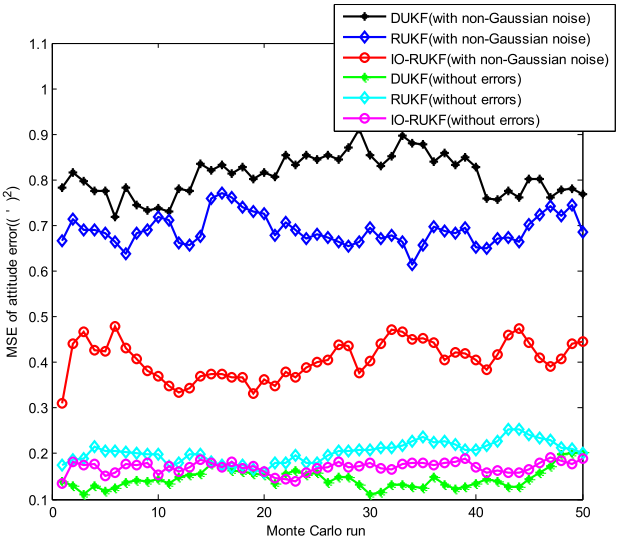

FIGURE 12. MSE of attitude error for the case with non-Gaussian measurement noise.

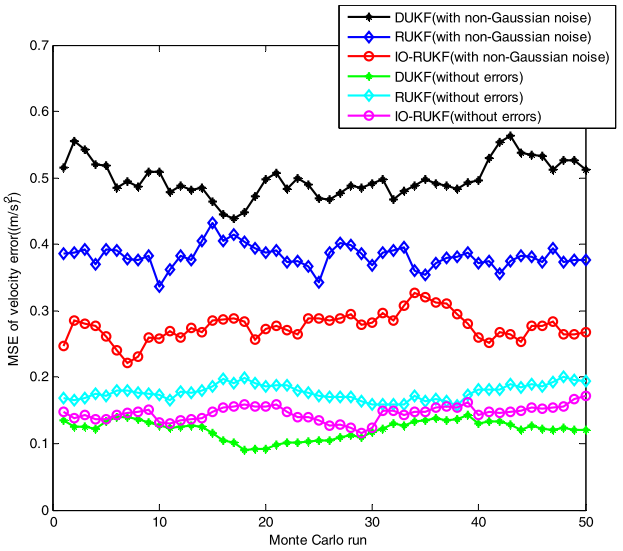

FIGURE 13. MSE of velocity error for the case with non-Gaussian measurement noise.

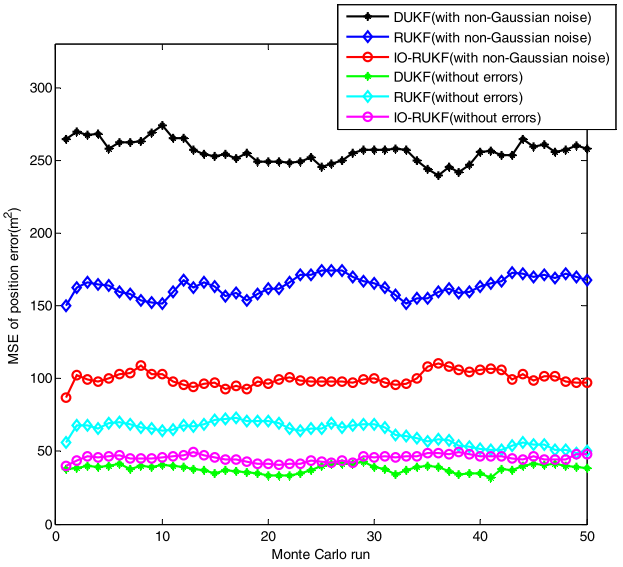

FIGURE 14. MSE of position error for the case with non-Gaussian measurement noise.

because the robust factor in IO-RUKF is obtained in an optimal manner, while the scaling factors in RUKF is determined empirically. In the time segments without the non-Gaussian noise, the simulation results of the three filters are similar to those in the case of observation outliers. Table 3 lists the mean overall errors in attitude, velocity and position for the times with the non-Gaussian measurement noise and the other time periods, which confirms the abovementioned phenomenon as well.

The MSEs of attitude error, velocity error and position error obtained by the DUKF, RUKF and IO-RUKF for the case with non-Gaussian measurement noise are depicted in Figs. 12∼14, which indicate the similar conclusion with the Figs. 9∼11. When the measurement noise is non-Gaussian, the DUKF is not robust, leading to the degraded navigation performance. Furthermore, compared to the RUKF, the proposed IO-RUKF has superior navigation accuracy due to the optimal determination manner of robust factors. For the time without non-Gaussian noise, the above three filters show the similar trend as in the case of observation outliers.

The above simulations and analysis demonstrate that the proposed IO-RUKF can effectively inhibit the influences of the measurement errors on system state estimation by using the robust factor to adjust the Kalman gain matrix, leading to the higher navigation performance than DUKF and RUKF for tightly coupled INS/GNSS integration for hypersonic vehicle navigation.

V. CONCLUSION

This paper presents a new IO-RUKF for tightly coupled INS/GNSS integration for hypersonic vehicle navigation. It addresses the disturbance on system state from

measurement errors caused by highly dynamic maneuvers of a hypersonic vehicle. The proposed IO-RUKF restrains the influences of measurement errors on the filtering solution by incorporating a robust factor to inflate the covariance of the predicted measurement and further decrease the Kalman gain such that the contribution of the measurements in error are less weighted to achieve the filtering robustness. Since the robust factor in the proposed IO-RUKF is derived based on the innovation orthogonality principle, it is optimal in theory, while the scaling factors in RUKF are determined empirically without consideration of optimality [26]. The simulation results and comparison analysis demonstrate that the proposed IO-RUKF has higher accuracy and robustness than DUKF and RUKF for tightly coupled INS/GNSS integration for hypersonic vehicle navigation.

Future research work will focus on enhancement of the presented IO-RUKF. The presented IO-RUKF will be extended to handle intermittent measurement data for hypersonic vehicle navigation.

REFERENCES

[1] B. Xu and Z. Shi, "An overview on flight dynamics and control approaches for hypersonic vehicles," *Sci. China Inf. Sci.*, vol. 58, no. 7, pp. 1–19, Jul. 2015.
[2] H.-L. Besser, D. Göge, M. Huggins, A. Shaffer, and D. Zimper, "Hypersonic vehicles—Game changers for future warfare?" *Transforming Joint Air Power: J. JAPCC*, vol. 24, pp. 11–27, Jul. 2017.
[3] P. Ouzts, D. Soloway, D. Moerder, D. Wolpert, and J. Benavides, "The role of guidance, navigation, and control in hypersonic vehicle multidisciplinary design and optimization," in *Proc. 16th AIAA/DLR/DGLR Int. Space Planes Hypersonic Syst. Technol. Conf.*, Bremen, Germany, 2009, p. 7329.
[4] C. Bahm, E. Baumann, J. Martin, D. Bose, R. Beck, and B. Strovers, "The X-43A Hyper-X Mach 7 flight 2 guidance, navigation, and control overview and flight test results," in *Proc. AIAA/CIRA 13th Int. Space Planes Hypersonics Syst. Technol. Conf.*, Capua, Italy, 2005, p. 3275.
[5] K. Chen, L. Y. Zhang, X. Wang, M. X. Liu, Y. F. Yu, and J. Yan, "Strapdown inertial navigation algorithm for hypersonic boost-glide vehicle," in *Proc. 21st AIAA Int. Space Planes Hypersonics Technol. Conf.*, Xiamen, China, 2017, p. 2174.
[6] G. Hu, W. Wang, Y. Zhong, B. Gao, and C. Gu, "A new direct filtering approach to INS/GNSS integration," *Aerosp. Sci. Technol.*, vol. 77, pp. 755–764, Jun. 2018.
[7] W. Wang, Z.-Y. Liu, and R.-R. Xie, "Quadratic extended Kalman filter approach for GPS/INS integration," *Aerosp. Sci. Technol.*, vol. 10, no. 8, 2006, pp. 709–713, 2006.
[8] J. L. Crassidis, "Sigma-point Kalman filtering for integrated GPS and inertial navigation," *IEEE Trans. Aerosp. Electron. Syst.*, vol. 42, no. 2, pp. 750–756, Apr. 2006.
[9] G. Hu, S. Gao, and Y. Zhong, "A derivative UKF for tightly coupled INS/GPS integrated navigation," *ISA Trans.*, vol. 56, pp. 135–144, May 2015.
[10] H. Carvalho, P. D. Moral, A. Monin, and G. Salut, "Optimal nonlinear filtering in GPS/INS integration," *IEEE Trans. Aerosp. Electron. Syst.*, vol. 33, no. 3, pp. 835–850, Jul. 1997.
[11] S. Y. Cho, "IM-filter for INS/GPS-integrated navigation system containing low-cost gyros," *IEEE Trans. Aerosp. Electron. Syst.*, vol. 50, no. 4, pp. 2619–2629, Oct. 2014.
[12] M.-J. Yu, "INS/GPS integration system using adaptive filter for estimating measurement noise variance," *IEEE Trans. Aerosp. Electron. Syst.*, vol. 48, no. 2, pp. 1786–1792, Apr. 2012.
[13] S. Gao, G. Hu, and Y. Zhong, "Windowing and random weighting-based adaptive unscented Kalman filter," *Int. J. Adapt. Control Signal Process.*, vol. 29, no. 2, pp. 201–223, Feb. 2015.
[14] J. Fang and X. Gong, "Predictive iterated Kalman filter for INS/GPS integration and its application to SAR motion compensation," *IEEE Trans. Instrum. Meas.*, vol. 59, no. 4, pp. 909–915, Apr. 2010.
[15] S. J. Julier and J. K. Uhlmann, "Unscented filtering and nonlinear estimation," *Proc. IEEE*, vol. 92, no. 3, pp. 401–422, Mar. 2004.
[16] G. Hu, S. Gao, Y. Zhong, B. Gao, and A. Subic, "Modified strong tracking unscented Kalman filter for nonlinear state estimation with process model uncertainty," *Int. J. Adapt. Control Signal Process.*, vol. 29, no. 12, pp. 1561–1577, Dec. 2015.
[17] S. Yazdkhasti, J. Z. Sasiadek, and S. Ulrich, "Performance enhancement for GPS/INS fusion by using a fuzzy adaptive unscented Kalman filter," in *Proc. 21st Int. Conf. Methods Models Automat. Robot.*, Miedzyzdroje, Poland, Aug./Sep. 2016, pp. 1194–1199.
[18] Y. Meng, S. Gao, Y. Zhong, G. Hu, and A. Subic, "Covariance matching based adaptive unscented Kalman filter for direct filtering in INS/GNSS integration," *Acta Astron.*, vol. 120, pp. 171–181, Mar. 2016.
[19] M.-M. Hu, Z. L. Jing, D. D. Peng, G. R. Zhou, and Z. M. Zheng, "Variational Bayesian filtering based on Student-t distribution for SINS/GPS integrated navigation," *J. ZheJiang Univ. (Eng. Sci.)*, vol. 52, no. 8, pp. 1482–1488, 2018.
[20] Q. Song and J.-D. Han, "An adaptive UKF algorithm for the state and parameter estimations of a mobile robot," *Acta Autom. Sinica*, vol. 34, no. 1, pp. 72–79, 2008.
[21] B. Gao, S. Gao, G. Hu, Y. Zhong, and C. Gu, "Maximum likelihood principle and moving horizon estimation based adaptive unscented Kalman filter," *Aerosp. Sci. Technol.*, vol. 73, pp. 184–196, Feb. 2018.
[22] W. Li and Y. Jia, "H-infinity filtering for a class of nonlinear discrete-time systems based on unscented transform," *Signal Process.*, vol. 90, no. 12, pp. 3301–3307, Dec. 2010.
[23] G. Chang, "Robust Kalman filtering based on Mahalanobis distance as outlier judging criterion," *J. Geodesy*, vol. 88, pp. 391–401, Jan. 2014.
[24] X. Wang, N. Cui, and J. Guo, "Huber-based unscented filtering and its application to vision-based relative navigation," *IET Radar Sonar Navigat.*, vol. 4, no. 1, pp. 134–141, Feb. 2010.
[25] L. Chang, B. Hu, G. Chang, and A. Li, "Robust derivative-free Kalman filter based on Huber's M-estimation methodology," *J. Process Control*, vol. 23, no. 10, pp. 1555–1561, 2013.
[26] Q. Wang and D. Xiao, "GPS/SINS positioning method based on robust UKF," in *Proc. Int. Conf. Ind. Control Electron. Eng.*, Xi'an, China, Aug. 2012, pp. 877–881.
[27] G. Arshal, "Error equations of inertial navigation," *J. Guid., Control, Dyn.*, vol. 10, no. 4, pp. 351–358, 1987.
[28] Y. Y. Qin, *Inertial Navigation*. Beijing, China: Science Press, 2006.
[29] P. S. Maybeck, *Stochastic Models, Estimation and Control*. New York, NY, USA: Academic Press, 1979.
[30] M. Boutayeb and D. Aubry, "A strong tracking extended Kalman observer for nonlinear discrete-time systems," *IEEE Trans. Autom. Control*, vol. 44, no. 8, pp. 1550–1556, Aug. 1999.
[31] G.-G. Hu, S.-S. Gao, Y.-M. Zhong, and B.-B. Gao, "Stochastic stability of the derivative unscented Kalman filter," *Chin. Phys. B*, vol. 24, no. 7, 2015, Art. no. 070202.

GAOGE HU received the B.S. degree in mathematics and applied mathematics and the Ph.D. degree in control theory and control engineering from Northwest Polytechnical University, Xi'an, China, in 2010 and 2016, respectively.

From 2016 to 2017, he was a System Engineer with Huawei Technologies Company Ltd. He is currently an Associate Professor with the School of Automation, Northwest Polytechnical University. His current research interests include integrated navigation, Kalman filtering, nonlinear state estimation, and multisensors data fusion.

BINGBING GAO received the Ph.D. degree in navigation, guidance, and control from Northwest Polytechnical University, Xi'an, China, in 2018. He is currently an Assistant Professor with the School of Automation, Northwest Polytechnical University. His research interests include information fusion, nonlinear filtering, and integrated navigation.

YONGMIN ZHONG is currently an Associate Professor with the School of Aerospace, Mechanical and Manufacturing Engineering, RMIT University, Australia. His research interests include computational engineering, haptics, soft tissue modeling, surgical simulation, aerospace navigation and control, intelligent systems, and robotics.

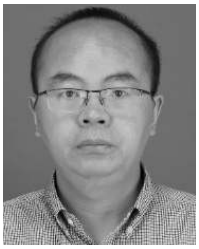

LONGQIANG NI received the M.S. and Ph.D. degrees in traffic information engineering and control from Northwest Polytechnical University, Xi'an, China, in 2008 and 2016, respectively. From 2003 to 2005, he was an Assistant Engineer with SINOPEC Yanshan Petrochemical Company, Beijing, China. In 2008, he was an Engineer with the Northwestern Institute of Mechanical and Engineering, Xianyang, China. He is currently an Associate Research Fellow. His research interests include navigation, control and decision making, nonlinear control, and sensor networks.

CHENGFAN GU research interests include bio/nano materials characterization and analysis, micro-forming, metallic materials processing, and computational modeling. She is a DECRA Fellow with the Australia Research Council, Australia.